Intensive *HST*, *RXTE* and *ASCA* Monitoring of NGC 3516: Evidence Against Thermal Reprocessing

Rick Edelson[1,2], Anuradha Koratkar[3], Kirpal Nandra[4,5], Michael Goad[2], Bradley M. Peterson[6], Stefan Collier[6], Julian Krolik[7], Matthew Malkan[1], Dan Maoz[8], Paul O'Brien[2], J. Michael Shull[9], Simon Vaughan[2], Robert Warwick[2]

ABSTRACT

During 1998 April 13–16, the bright, strongly variable Seyfert 1 galaxy NGC 3516 was monitored almost continuously with *HST* for 10.3 hr at ultraviolet wavelengths and 2.8 d at optical wavelengths, and simultaneous *RXTE* and *ASCA* monitoring covered the same period. The X-ray fluxes were strongly variable with the soft (0.5–2 keV) X-rays showing stronger variations ($\sim$65% peak-to-peak) than the hard (2–10 keV) X-rays ($\sim$50% peak-to-peak). The optical continuum showed much smaller but still highly significant variations: a slow $\sim$2.5% rise followed by a faster $\sim$3.5% decline. The short ultraviolet observation did not show significant variability.

The soft and hard X-ray light curves were strongly correlated with no evidence for a significant interband lag. Likewise, the optical continuum bands (3590 Å and 5510 Å) were also strongly correlated with no measurable lag to 3σ limits of $\lesssim$0.15 d. However, the optical and X-ray light curves showed very different behavior, and no significant correlation or simple relationship could be found. These results appear difficult to reconcile with previous reports of correlations between X-ray and optical variations and of measurable lags within the optical band for some other Seyfert 1s.

These results also present serious problems for "reprocessing" models in which the X-ray source heats a stratified accretion disk which then reemits in the optical/ultraviolet: the synchronous variations within the optical would suggest that the emitting region is $\lesssim$0.3 lt-d across, while the lack of correlation between X-ray and

[1]Astronomy Department; University of California; Los Angeles, CA 90095-1562; USA

[2]X-ray Astronomy Group; Leicester University; Leicester LE1 7RH; United Kingdom

[3]Space Telescope Science Institute; 3700 San Martin Dr.; Baltimore, MD 20771; USA

[4]NASA/Goddard Space Flight Center; Laboratory for High Energy Astrophysics; Code 662; Greenbelt, MD 20771; USA

[5]Universities Space Research Association

[6]Astronomy Department; Ohio State University; 180 W. 18th Ave.; Columbus, OH 43210-1173; USA

[7]Department of Physics and Astronomy; The Johns Hopkins University; Baltimore, MD 20771; USA

[8]School of Physics & Astronomy and Wise Observatory; Tel-Aviv University; Tel-Aviv 69978; Israel

[9]Center for Astrophysics and Space Astronomy; University of Colorado; Boulder, CO 80309; USA

optical variations would indicate, in the context of this model, that any reprocessing region must be $\gtrsim$1 lt-d in size. It may be possible to resolve this conflict by invoking anisotropic emission or special geometry, but the most natural explanation appears to be that the bulk of the optical luminosity is generated by some other mechanism than reprocessing.

Subject headings: galaxies: active — galaxies: individual (NGC 3516) — galaxies: Seyfert — optical: galaxies — X-rays: galaxies

1. Introduction

Seyfert 1 galaxies emit substantial luminosity over $\sim$8 decades of frequency, from the far-infrared through the hard X-rays. As this is much too broad to be from a single thermal source, this indicates that there must be nonthermal (e.g., synchrotron or inverse-Compton) and/or multiple emission components. Comparison between variations in different wavebands can distinguish between these possibilities and, in the latter instance, establish relationships between different components. A well-sampled 1 month campaign of simultaneous *International Ultraviolet Explorer* (*IUE*) and *Rossi X-ray Timing Explorer* (*RXTE*) monitoring of the Seyfert 1 NGC 7469 found similar overall amplitudes in both bands, but the X-rays had much stronger short term variations, and correlated interband variability could not be detected (Nandra et al. 1998). Done et al. (1990) found that NGC 4051 showed no measurable optical variations during a 3 d period in which strong X-ray variations were seen. Recent contemporaneous *RXTE*/optical observations of NGC 3516 over a 500 d period (Maoz, Edelson & Nandra 1999) also failed to detect clear interband correlation. On the other hand, apparent correlations between optical/ultraviolet and X-ray variations had been claimed in earlier, less well-sampled observations of NGC 4151 (Edelson et al. 1996) and NGC 5548 (Clavel et al. 1992). These contradictions indicate that the nature of the relationship between X-ray and lower energy variations remains to be clarified.

A similar issue is the relation between variations in hard and soft X-ray bands. In a recent *Advanced Satellite for Astronomy and Cosmology* (*ASCA*) survey, Nandra et al. (1997) found some cases in which the variability amplitudes at soft X-ray energies were larger than those in the hard X-rays (see also Turner et al. 1999), but these observations were too short to estimate interband lags. However, in simultaneous *Extreme Ultraviolet Explorer* (*EUVE*), *ASCA* and *RXTE* monitoring of NGC 5548 and MCG–6-30-15, Chiang et al. (1999) and Reynolds (1999) respectively reported evidence that the variations at softer X-ray energies consistently led those at harder X-ray energies. If confirmed, causality arguments would require rejection of "reprocessing" models in which the soft X-rays are "secondary" emission produced by passive reradiation of "primary" hard X-ray photons in, e.g., an accretion disk.

Finally, the same arguments apply to variations within the optical/ultraviolet as well. Early studies found no evidence for lags between variations within the ultraviolet and optical bands, to

a limit of $\lesssim$1 d in NGC 5548 (Krolik et al. 1991, Korista et al. 1995) and $\lesssim$0.2 d in NGC 4151 (Edelson et al. 1996). The recent NGC 7469 campaign data suggested evidence for progressively longer lags, from 0.3 to 1.8 d, between variations at 1315, 1825, 4845 and 6962 Å (Wanders et al. 1997, Collier et al. 1998). Peterson et al. (1998) then reanalyzed the optical/ultraviolet data for NGC 4151 (Kaspi et al. 1996) and reported similar evidence that the shortest wavelength ultraviolet variations preceded those at the longest optical wavelengths, albeit at a lower confidence level. These time lags have been interpreted in models in which the ultraviolet is reprocessed in an accretion disk to optical photons (Collier et al. 1998).

This paper presents the results of simultaneous X-ray, ultraviolet and optical observations of NGC 3516, a bright Seyfert 1 galaxy, designed to address these issues by sampling much faster than any previous Seyfert 1 monitoring campaign. The observations and data reduction are discussed in the next section. The variability amplitudes and interband lags were then measured, as discussed in §§ 3 and 4. Surprising evidence was found that the optical showed small variations that occurred simultaneously within the optical band (to within $\lesssim$0.15 d) and that were not simply related to the much larger X-ray variations. The theoretical implications of these results are discussed in § 5, followed by a summary of the paper's main results in § 6.

2. Observations and Data Reduction

Simultaneous observations were made of NGC 3516 with *RXTE*, *ASCA* and *Hubble Space Telescope* (*HST*) on 1998 April 13–16. This bright ($m_v = 12.5$), strongly variable Seyfert 1 nucleus resides in an SB0 galaxy at redshift $z = 0.0088$. NGC 3516 is a northern source ($\delta = +72^\circ$) that lies near the pole of the orbit of *HST*, making it the only bright Seyfert 1 galaxy over which the "continuous viewing zone" (CVZ) passes at some time during the year. (The position of the CVZ changes as the satellite's orbit precesses.) NGC 3516 was visible without interruption during two periods in 1998. The *RXTE* CVZ also passes over NGC 3516 and in fact this source was in the CVZs of *both HST* and *RXTE* in 1998 February, but STScI was unable to schedule the *HST* observations. Even so, NGC 3516 was in the *HST* CVZ during the 1998 April observations and the *RXTE* on-source efficiency was also relatively good.

2.1. RXTE Data

RXTE observed NGC 3516 from 1998 April 13 08:01:08 to April 16 16:10:44 UT. The current study is restricted to Proportional Counter Array (PCA), `STANDARD-2`, 2–10 keV, Layer 1 data because that is where the PCA is best calibrated and most sensitive. Because Proportional Counter Units (PCUs) 3 and 4 were occasionally turned off, only data from the other three PCUs (0, 1 and 2) were used. Good quality data were accepted on the basis of the following criteria: the satellite was outside the South Atlantic Anomaly (SAA), the Earth elevation angle was $\geq 10^\circ$,

the offset from the nominal optical position was $\leq 0\overset{\circ}{.}02$, and ELECTRON-O was ≤ 0.1. The last criterion removes data with high particle background rates in the PCUs, and the first censors data with high induced particle count rates, both of which are conditions under which the background model is relatively unreliable. After screening, the total amount of good data was 142.9 ks. Background subtraction was performed using the L7-240 model, but the systematic errors are still large ($\sim$0.15 ct s^{-1}). These dominate the uncertainties on all but the shortest time scales. See Edelson & Nandra (1999) for further details of the reduction procedure as well as a discussion of the *RXTE* PCA background.

Light curves were initially extracted with 16 s time resolution. The data were rebinned on the orbital sampling period (5760 s), with the Earth-occultation gaps as the bin edges. This has the advantage of improving the signal-to-noise and sampling the light curve on the shortest available uninterrupted time scale. The distribution of the $\gtrsim$200 individual points within each bin was used to assign standard errors and mean count rates for each orbit. Thus, these quantities included statistical errors appropriate to variability measurement but not systematic effects such as overall calibration errors that would be appropriate to spectroscopy. The resultant light curve is shown in Figure 1.

2.2. ASCA Data

ASCA observed NGC 3516 from 1998 April 12 22:30:01 to April 17 04:54:01 UT. All four detectors were in operation, although here only data from the Solid-state Imaging Spectrometers (SIS) are considered. These were analyzed using standard methods; for further details see Nandra et al. (1999). Source counts were extracted from a region centered on NGC 3516 with a radius of $4\overset{'}{.}7$. Data were combined from the two SIS instruments to produce a mean light curve, selecting times only when both instruments were deemed to be collecting data of good quality. Data were rejected when the angular distance between the pointing position and the nominal source position exceeded $0\overset{\circ}{.}01$, when the satellite was passing through the SAA and 16 s thereafter, when the Earth elevation angle was less than 10° (20° for the bright Earth), when the cut-off rigidity was less than 6 GeV/c, when the count rate of the radiation-belt monitor (RBM_CONT) exceeded 500 ct s^{-1}, when the pixel number over the threshold (Sn_PIXLn) in the nominal chip exceeded 100, or during the 16 s after the satellite passed the day-night terminator. Hot and flickering pixels were cleaned from the images using standard techniques. Light curves were extracted in 128 s bins in both the hard (2–10 keV) and soft (0.5–2 keV) bands. The *ASCA* data were not background subtracted because the flux from the source filled most of the chip. We estimate the background contribution to the light curves to be no more than a constant $\sim$3%. There is no evidence that the SIS background is variable on the time scales sampled here, so this made a negligible contribution to the overall error and fractional variability level estimates. These data were rebinned by *ASCA* orbit, as described above for the *RXTE* data. The resultant light curves are shown in Figure 1.

2.3. HST Ultraviolet Data

HST observed NGC 3516 separately with the Space Telescope Imaging Spectrometer (STIS) UltraViolet Micro-Anode Multichannel Array (UV-MAMA) and optical-CCD, covering the wavelength ranges 1150–1736 Å and 2900–5700 Å respectively. Because of STIS MAMA limitations (it cannot be used during SAA passages), the ultraviolet observations were conducted only during a single SAA-free period: 1998 April 13 07:55:14 to 18:17:37 UT. The G140L grating (1150–1736 Å) was used in time-tagged mode with a $52'' \times 0\farcs5$ slit for a total exposure time of 32.8 ks. To maximize the period in the CVZ, the observations were obtained using the smaller bright Earth limb avoidance angle of 16°. (The increased airglow-induced background is negligible in the UV-MAMA.) NGC 3516 was re-acquired at the beginning of each orbit but no wavelength calibration (WAVECAL) observations were obtained in order to allocate as much time as possible to integration on the target.

The time-tagged data were converted into 6 min integrated images, then calibrated with CALSTIS v2.0, using the reference files that were closest in time (and, as it happens, were also the best available). The 2-dimensional data were calibrated and extracted into 1-dimensional spectra with a 7 pixel extraction ($0\farcs35$) window. The relative wavelength calibration accuracy was determined by registering Galactic C II (1334.53 Å) and Si II (1526.71 Å) in the orbitally-averaged data. There was a maximum motion of 0.3 and 0.2 pixels for the C II and Si II lines, respectively, and the 1σ variation in the line centers was 0.17 pixel, which corresponds to 0.1 Å. The zero point wavelength calibration uncertainty was ∼0.7 pixel (0.4 Å).

Fluxes were extracted for the 1355–1365 Å continuum band and C IV emission line and then light curves were determined by measuring the mean and standard error on the ∼15 individual 6 min data points in each *HST* orbit, in an analogous fashion to the X-ray light curves discussed above. The resulting light curves are shown in Figures 1 and 2 and the mean spectrum, indicating the continuum bands used in the light curve, is shown in Figure 3.

There are a number of possible systematic effects that could affect the relative flux calibration, including thermal fluctuations, wavelength drift, spacecraft stability and pointing. In particular, the G140L flux measurement is a function of temperature due to thermal motion of the target (ISR/STIS 98-27). This effect is not corrected for in the pipeline re-calibration and the temperature variation seen in these data is 4.05°C, which corresponds to a systematic change of 1.5% in flux. As discussed in § 3, this can probably account for a large fraction of the apparent variability in this relatively short observation.

2.4. HST Optical Data

Optical spectra were obtained every 3 min using the STIS CCD/G430L grating and the $52'' \times 0\farcs5$ slit from 1998 April 13 21:58:11 to April 16 16:59:09 UT. Four orbits were lost due

to spacecraft/instrument problems, yielding a total optical exposure time of 138.2 ks. As with the UV-MAMA observations, all observations were obtained using the smaller bright Earth limb avoidance angle of 16°, and no WAVECALs were taken in order to increase the on-target integration time. The increased airglow-induced background can be effectively corrected for in the CCD/G430L grating.

As with the STIS MAMA data, the STIS CCD data were calibrated and extracted into 1-dimensional spectra with a 7 pixel extraction (0.″35) window. The 1-dimensional spectra were measured as both 3 min and orbital averages. The 3 min data were used to measure continuum fluxes and errors in the same fashion as with the previous data sets, but this was not done for the line fluxes because wavelength drift would have required manually adjusting the wavelength scales for almost 1,000 spectra. Instead, wavelength adjustment was performed for the 38 orbitally-averaged spectra using Galactic lines. Initially, the 1σ variation was 0.17 pixels (0.46 Å), and the maximum motion was 0.6 pixels (1.6 Å). After wavelength correction the maximum motion in the lines was 0.031 pixels (0.08 Å). These data were used to measure the line fluxes, but because the orbitally-averaged data were used, errors were not estimated.

STIS CCD observations were performed in ALONG-SLIT mode. This involved trailing the source parallel to the slit (that is, in the spatial direction) to enable clean removal of bad pixels and cosmic-ray events. Superposed on this motion of the source along the slit were additional small (±0.5 pixel) motions perpendicular to the slit axis (that is, in the dispersion direction), as a consequence of dithering of the parallel Wide Field/Planetary Camera (WFPC2) observations. These were performed to reduce the effects of small-scale non-uniformity in the WFPC2 detector, increasing the dynamic range and effective spatial resolution of the WFPC2 observations. We have investigated the effects of this dithering and find that there is no systematic relation between the position and either continuum or line fluxes, so the dithering is not a likely source of systematic error.

In the calibrated spectra, fluxes were measured for the 3575–3600 Å, 4223–4245 Å, 5500–5525 Å continuum bands and [O III] (5137–5255 Å), Hβ (4861–4946 Å) and Hγ (4350–4430 Å) emission lines. In addition, mean optical continuum fluxes (defined as the harmonic mean of the fluxes in the three continuum bands) and mean line fluxes (the harmonic mean of the three line fluxes) were also determined for each orbit. These light curves are presented in Figures 1 and 2 and the mean spectrum is presented in Figure 4.

Narrow band images of NGC 3516 in [O III] (4959 and 5007 Å) show a biconical extended (5″) emission-line region with position angle of 25° (Golev et al. 1995). Due to roll angle constraints, the STIS aperture was aligned at position angle 98°. The slit position is almost perpendicular to the extended narrow emission-line region. This means that in principle, small variations could be induced in the derived narrow emission-line flux due to variations in spacecraft roll angle ($\sim 2°$ maximum), although the [O III] light curve shows no evidence of excess scatter (e.g., above that seen in the Balmer lines), so this is apparently not a problem.

3. Variability Amplitudes

To quantify the amplitude of variations in different bands, we computed the fractional excess variance, σ^2_{XS}, defined as

$$\sigma^2_{XS} = \frac{S^2 - \langle\sigma^2_{err}\rangle}{\langle X\rangle^2}, \tag{1}$$

where $\langle X\rangle$ is the mean flux, $\langle\sigma^2_{err}\rangle$ is the mean square error, and S^2 is the measured variance of the light curve (see Nandra et al. 1997). It is intended as a measure of the intrinsic source variability power during a given time interval, corrected for the effects of measurement noise and normalized to the mean flux. No error has been estimated for the emission line measurements, so the quoted values of σ^2_{XS} are in these cases upper limits.

Table 1 summarizes these results for the X-ray, ultraviolet and optical data. It shows that the X-rays were strongly variable, and that the fractional excess variance measured with both *RXTE* and *ASCA* in the hard X-ray band (2–10 keV) is smaller than that measured in the softer X-ray band (0.5–2 keV) with *ASCA*. The larger soft band variability is also apparent in Figure 1.

The optical/ultraviolet continuum variations were much weaker than those in the X-rays. In the optical, the excess variance in the continuum is approximately twice that measured in the [O III] and Hβ lines and 50% larger than that in the Hγ line. Furthermore, the apparent variations in the lines are not coherent, but those in the continuum are, with all three continuum bands showing a slow rise of $\sim$2.5% followed by a faster decline of $\sim$3.5%. This behavior is not seen in any of the emission line light curves. The key independent test is provided by the mean emission line light curve. It is completely flat, with an RMS standard deviation of 0.26%. We conclude that the systematic errors are no larger than this. This in turn indicates that these small optical continuum variations are real. While these would be improbably small errors for ground-based observations, we note that previous observations have demonstrated that *HST* is capable of such high-precision monitoring (e.g., Welsh et al. 1998).

In the ultraviolet, σ^2_{XS} is somewhat larger for the C IV line than for the 1360 Å continuum. It is unlikely that C IV would vary by this large an amount ($\sim$5% peak-to-peak) in 10 hr; furthermore, the line and continuum light curves have very similar shapes. Also, as discussed in § 2.3, the ultraviolet data suffer from instabilities not seen in other bands (in particular, detector gain changes induced by thermal variations). This all suggests that the ultraviolet continuum variability could very likely have resulted from systematic effects not included in the measured (statistical) errors. Thus, we are forced to conclude that these data do not give unambiguous evidence of significant ultraviolet variations.

4. Interband Correlations

In order to further examine the relation between variations in different bands, temporal cross-correlation functions were measured using both the interpolated correlation function (ICF; White & Peterson 1994) and the discrete correlation function (DCF; Edelson & Krolik 1989). Errors on the ICF lags were estimated using the bootstrap method of Peterson et al. (1998).

4.1. Correlations Within the X-Rays

Within the hard X-ray band (2–10 keV), the *RXTE* and *ASCA* light curves were highly correlated ($r = +0.97$) with no hint of any lag. A zero-lag correlation diagram for these data is shown in Figure 5. The smaller error bars and higher count rates indicate that in this band, *RXTE* is the superior satellite for monitoring bright Seyfert 1s like NGC 3516. The very good correlation indicates that systematic errors in the background model to not significantly affect either data set.

Figure 6 shows the temporal cross-correlation functions between the two X-ray bands (top), within the optical (middle) and between the optical and X-rays (bottom). The *RXTE* hard – *ASCA* soft ICF reaches a maximum correlation coefficient of $r_{max} = +0.95$ for a lag of $\tau = -0.02$ d. The two highest points in the DCF are at zero lag and –1 orbit (–0.067 d), and a smoothed parabolic fit is centered on $\tau = -0.020^{+0.018}_{-0.022}$ d (in the sense that the *RXTE* hard X-ray variations would lead the *ASCA* soft X-ray variations). These values are less than half of a single orbital bin and we consider this result to be consistent with the null hypothesis, that is, that there is no measurable interband lag with a 3σ limit of $\tau \lesssim 0.07$ d.

4.2. Correlations Within the Optical

No significant lag was seen within the optical band either. Along the longest wavelength baseline, 3590 – 5510 Å, the DCF peaked at zero lag and the ICF centroid was $\tau = -0.012^{+0.053}_{-0.052}$ d (see Figure 6). Likewise, over the 3590 – 4235 Å baseline, the DCF peaked at zero lag and the ICF centroid was at $\tau = -0.002^{+0.035}_{-0.047}$ d (not shown). In both cases, the correlation is strong ($r_{max} = 0.906$ and 0.944, respectively). The 3σ upper limits on any possible lags are $\tau \lesssim 0.15$ d.

4.3. Correlations Between X-ray and Optical Variations

The peak in ICF for the hard X-ray (*RXTE* 2–10 keV) and mean optical continuum light curves is at $\tau = -0.21^{+0.07}_{-0.34}$ d, but the maximum correlation coefficient is only $r_{max} = +0.53$ (see Figure 6). This would be significant at the $P \approx 0.0008$ level if it was the result of only one trial, and if the data were all independent. Because there were 38 trials, the significance is lower and P must be multiplied by 38, yielding $P \approx 3\%$. Furthermore, the red noise character of the

fluctuation Power Density Spectra (PDS) means that the measurements are not independent. This, in turn means that the (already marginal) significance must be further reduced (see Maoz et al. 1999). Monte-Carlo simulations indicate that the corrected probability is $P \approx 24\%$, which is not significant. In fact, the most significant value of r is the *anticorrelation* with $r_{min} \lesssim -0.8$ for $\tau = +0.6$ to $+1.3$ d. This anticorrelation is certainly not predicted by any model, and the fact that it is so broad further suggests that it is a spurious effect as discussed above. Thus, we must conclude that these data contain no clear evidence for correlated X-ray/optical variability.

To sum up these results, the optical and X-ray variations show no significant interband correlation, while within each of the bands, the intraband variations are highly correlated with no measurable delays longer than the strong upper limits of a few hours. These findings have important physical implications, as discussed below.

5. Discussion

5.1. Reprocessing Models

Much attention has been given to reprocessing models for the optical emission from Seyfert 1 galaxies in which an X-ray continuum source irradiates relatively dense and cool material which, in turn, emits thermal radiation at longer (optical/ultraviolet) wavelengths (e.g., Guilbert & Rees 1988, Rokaki et al. 1992). There is a good body of X-ray spectral evidence in support of this model: many Seyfert galaxies show evidence for a strong "Compton bump" in the X-ray spectrum, a signature of reflection from an absorbing medium (Lightman & White 1988, Pounds et al. 1990, George & Fabian 1991). Any absorbed X-ray flux must also be re-emitted. A likely candidate for the putative absorber (but not the only one, e.g., Krolik et al. 1994, Ghisellini et al. 1994) is thermally-emitting matter close to the central black hole (e.g., an accretion disk). Any such thermalizing source should radiate in the optical/ultraviolet. There is also a strong theoretical prejudice that the primary energy release should occur just outside the marginally stable orbit around a black hole as the result of flow through an accretion disk. It is plausible that both the X-ray and optical/ultraviolet source could be located in that vicinity. Moreover, specific Comptonization models making use of this geometry result in rough agreement with observed spectra (e.g., Haardt & Maraschi 1991).

This model (and any other involving a central driver, e.g., Krolik et al. 1991, Clavel & Courvoisier 1991) has important implications for the variations seen in the optical continuum. On time scales longer than the light-crossing time of the reprocessing region, the optical/ultraviolet variations should follow those in the (driving) X-ray band, but at shorter time scales, they should be smoothed out by light travel-time effects. Because most of the short-wavelength optical/ultraviolet continuum arises at smaller radii than most of the longer-wavelength continuum, this model also implies a time delay between the variations at short and long wavelengths.

The details of both the "smearing" of rapid fluctuations and the interband delays depend on details of the system's structure. However, their general character may be illustrated by a simple model: Suppose that most of the flux at wavelength λ is thermal radiation from material with temperature $T \sim hc/(k\lambda)$, (e.g., as in a conventional accretion disk) where h, c and k are physical constants. Then the area of this region is $A \sim \lambda L_\lambda/(\sigma T^4)$, where L_λ is the luminosity at that wavelength and σ is a physical constant, and the associated length scale is $R \propto (\lambda L_\lambda)^{1/2}\lambda^2$. If the signal propagation speed is v_s ($= c$ in a reprocessing model), both the most rapid fluctuation that can be reproduced at wavelength λ and the delay at that wavelength are of order

$$\tau(\lambda) \sim R/v_s \sim \sigma^{-1/2}\left(\frac{k}{hc}\right)^2\left(\lambda^5 L_\lambda\right)^{1/2}. \quad (2)$$

For an externally irradiated accretion disk, the luminosity emitted per unit area is proportional to R^{-3} and the temperature distribution is $L_\lambda \propto \lambda^{-7/3}$, so that $\tau \propto \lambda^{4/3}$. Moreover, if the central source luminosity is proportional to the accretion rate, then $\tau \propto R \propto (M\dot{M})^{1/3}$ (Shakura & Sunyaev 1973). Combining these, the overall relation is $\tau \propto (M\dot{M})^{1/3}\lambda^{4/3}$ (Collier et al. 1998, Peterson et al. 1998).

5.2. NGC 3516 and NGC 7469

Time delays of this sort have in fact been reported in the Seyfert 1 galaxy NGC 7469 (Wanders et al. 1997, Collier et al. 1998). Other multiwavelength monitoring programs have generally not been sufficiently well sampled or of sufficient duration (or both) to expect detection of these delays, although there is marginal evidence for such a lag between the shortest-wavelength ultraviolet and the longest-wavelength optical continuum bands in NGC 4151 (Peterson et al. 1998). The lags are roughly consistent with the predicted relation $\tau \propto (M\dot{M})^{1/3}\lambda^{4/3}$. However, even in NGC 7469, the magnitudes of relative continuum lags $\tau = 0.36^{+0.11}_{-0.17}$ d between 1315 Å and 1825 Å, and $\tau = 1.7^{+1.1}_{-0.8}$ d between 1315 Å and 6962 Å (Kriss et al. 1999), are uncomfortably close to the mean sampling of the light curves (0.17 d in the ultraviolet and 1.0 d in the optical).

Fitting the $\tau \propto \lambda^{4/3}$ relation to the NGC 7469 data (as done by Collier et al. 1998) yields a predicted lag between 3590 Å and 5510 Å of $\tau = 0.55 \pm 0.27$ d. If the central mass can be estimated from the formula $M \propto v^2\tau_e$ (e.g., Peterson & Wandel 1999), where v is the broad line velocity width and τ_e the emission-line lag, then the ratio of virial masses NGC 7469 and NGC 3516 is $M_{3516}/M_{7469} = 0.29$. Furthermore, if the accretion rate scales as the luminosity, $L_{3516}/L_{7469} = \dot{M}_{3516}/\dot{M}_{7469} = 0.50$. This crude scaling predicts the relative time delay between the 3590 Å and 5510 Å variations of NGC 3516 will be $\tau = 0.28$ d. Although this way of estimating $M\dot{M}$ is very uncertain, relatively large uncertainties can be tolerated because the dependence of τ on $M\dot{M}$ is so weak.

Alternatively, one could assume that the bolometric luminosity has a fixed ratio to the ultraviolet luminosity, and that the Eddington ratio L/L_E is the same in NGC 3516 as in

NGC 7469. In this case, $\tau \propto L^{2/3}$, which predicts that the relative time delay between the 3590 Å and 5510 Å variations of NGC 3516 will be $\tau = 0.31$ d.

Hence, the observed upper bound of $\tau \lesssim 0.15$ d in NGC 3516 appear inconsistent with the predicted value. However, it is unclear how much stress should be laid upon this conflict, given the numerous model dependencies built into the derivation and the fact that the NGC 7469 result is thus far unique and less than definitive. it should be noted that a similar discrepancy would have been found upon comparison with almost any conventional accretion disk model.

5.3. Implications for X-ray/Optical Correlations

The combination of a lack of measurable correlation between the X-ray and optical light curves and the synchronicity within the optical band presents even more serious general problems for the reprocessing model discussed above, independent of any possible disagreements between the scaling from the NGC 7469 results. The problem is that each of these results implies a limit on the size of the reprocessing region that is incompatible with the other.

The lack of response to the X-rays indicates that the light-crossing time of the optical/ultraviolet reprocessing region is of order or larger than the duration of the simultaneous X-ray/optical monitoring. Otherwise, the light curves should show some correlation if the optical/ultraviolet is in fact driven by the X-rays. Since this experiment ran 2.8 d, this would indicate that the reprocessing region would have to be $\gtrsim$1 lt-d in size. In fact, much longer term monitoring also failed to show the X-rays leading the optical variations, on delay time scales of weeks to months (Maoz et al. 1999). This in fact indicates that the reprocessing region should be light-weeks across or larger.

On the other hand, the observation of significant optical variability with no lags between the bands down to time scales of $\lesssim$0.15 d yields an upper limit on the size of the reprocessing region. For the most straightforward geometry, this upper limit in the lag yields an upper limit on the radius of the emitting region. Assuming the relation derived earlier for the stratified temperature structure of an externally-irradiated α-disk (Shakura & Sunyaev 1973), $T \propto R^{-3/4}$. By Wein's law, $T \propto 1/\lambda_{max}$, so $R \propto \lambda_{max}^{4/3}$. For a ratio of peak wavelengths 3590 Å/5510 Å, the ratio of the distances of the rings emitting most strongly at 3590 Å and 5510 Å is 1.9, that is, the radius of the 5510 Å-emitting ring is 1.9 times that of the 3590 Å-emitting ring. An upper limit of $\lesssim$0.15 lt-d for the distance between them corresponds to an upper limit of $\lesssim$0.3 lt-d for the radius of the entire system. Furthermore, if the optical continuum is produced in the same region as the iron Kα line, the relativistic effects observed in the line profile of NGC 3516 (Nandra et al. 1999) would also argue for an origin much closer to the central source. Thus, quite independent of the conflict with an extrapolation of any NGC 7469 result, these data create difficulties for the simplest reprocessing models.

There are a number of ways to get around this contradiction. One possible explanation is

that the flux of X-rays striking the disk is too small to significantly affect its output. The observed monochromatic luminosity at 3590 Å is about twice that at 2 keV, but since the X-ray variability amplitude is ∼20 times that in the optical, the variable monochromatic power in the X-rays is ∼10 times that in the optical. However, the scaling of the monochromatic to integrated luminosities of the X-ray and optical/ultraviolet components are not well-determined, and this may decrease this ratio. Even if the X-ray luminosity is great enough to affect the optical, it might be that most of the X-rays are actually directed away from the disk, e.g., if the solid angle subtended by the disk seen by the X-ray source is small (Dove et al. 1997) or if it is moving away from it at relativistic speeds (Beloborodov 1999). However, all of these models contradict the assumption that the observed optical variations are driven by the variable X-ray source.

Another possibility is that the reprocessor is smooth, but that the X-ray source is patchy, flaring and of non-negligible size compared to the reprocessor (Stern et al. 1995). There is some evidence for this, especially the scale-free character of the short term X-ray variability (e.g., McHardy & Czerny 1987), which argues against a single, coherent source. In this case, because the geometry is so complex, the temporal relation between variations cannot be easily predicted.

However, it may be that the most natural explanation is simply that the optical and X-ray-emitting regions are powered primarily by different processes. In this case, there is no reason to assume that a central source drives the stratification of the putative disk, so individual regions can change brightness independently, and the low-amplitude optical fluctuations could be due to a modulation in the luminosity of regions that do not dominate the total flux in these bands. For example, if only a single region varied, one would expect progressively larger fractional amplitudes of variation toward shorter wavelength (as is, in fact, generally observed; Edelson, Krolik & Pike 1990), and these variations would be simultaneous, as observed.

Finally, these results are consistent with the claims of no clear ultraviolet/X-ray correlation in NGC 7469 (Nandra et al. 1998) and longer-term optical/X-ray monitoring of NGC 3516 (Maoz et al. 1999). The earlier claims of significant correlations between X-ray and optical/ultraviolet variations in NGC 5548 (Clavel et al. 1992) and NGC 4151 (Edelson et al. 1996) may have been due to the "red-noise" character of the variations (see, e.g., Edelson & Nandra 1999), which can lead to an overestimate of the significance of a measured correlation (Maoz et al. 1999).

5.4. Hard/Soft X-ray Variability

The overall appearance of the variations in the soft and hard X-ray bands was similar, with no significant measurable lag between bands. However, the soft X-rays were a factor of ∼30% more strongly variable than the hard X-rays.

As noted in the introduction, there have recently been claimed measurements of phase differences (lags) between variations in hard and soft X-rays, with the soft X-rays leading the hard X-rays by ∼0.06 d in NGC 5548 (Chiang et al. 1999) and by ∼0.001 d in MCG–6-30-15 (Reynolds

1999, Lee et al. 1999). These are ∼0.9 and 0.02 times the fundamental orbital sampling rate. No error estimates were reported, although subsequent analysis yielded an error estimate of $^{+0.03}_{-0.05}$ d on the NGC 5548 lag (Nowak, priv. comm.).

In the current work, we estimated that the lag was not significantly different from zero, as the hard (2–10 keV) X-rays were seen to lead the softer (0.5–2 keV) X-rays by $0.020^{+0.018}_{-0.022}$ d. That is, the most likely lag seen in NGC 3516 is in the *opposite* sense as that reported for NGC 5548 and MCG–6-30-15. If real, this would seem to suggest that not all Seyfert galaxies exhibit the same type of temporal relationship between hard and soft X-ray variations. It is not clear what physical process could produce such behavior.

6. Conclusions

This paper reports the results of the most intensive multiwavelength Seyfert 1 monitoring campaigns ever undertaken: continuous, simultaneous monitoring of the Seyfert 1 galaxy NGC 3516 once every ∼96 min, at optical, soft X-ray and hard X-ray wavelengths, obtained with *HST*, *ASCA* and *RXTE* respectively, over a 2.8 d period. The *HST* data were repeatable at the $\lesssim$0.26% level or better. The observational results were:

1. The X-ray variations were very strong, ∼65% peak-to-peak in the soft X-ray band (0.5–2 keV) and ∼50% in the hard X-ray band (2–10 keV). These light curves were highly correlated ($r = 0.95$), with no measurable interband lag to 3σ limits of $\tau \lesssim 0.07$ d.

2. The optical continuum bands showed small but significant variations: a slow ∼2.5% rise followed by a faster ∼3.5% decline. The variations were highly correlated across the optical continuum bands ($r \geq 0.9$), with no measurable interband lag (to a 3σ limit of $\tau \lesssim 0.15$ d between 3590 Å and 5510 Å).

3. Temporal cross-correlation functions gave no evidence for a simple relation between the X-ray and optical variations. The most significant value was the anticorrelation of $r \lesssim -0.8$ for $\tau = -0.8$ to –1.3 d and the maximum positive correlation of $r = +0.53$ at $\tau = -0.21$ d, which was not deemed significant after accounting for interdependence of the data.

4. The optical emission lines showed no evidence for variability: a light curve constructed by averaging [O III], Hβ and Hγ line fluxes was flat with 0.26% RMS dispersion. Likewise, ∼5% variations seen during the short preceding ∼10 hr ultraviolet observation were not deemed significant as they are most likely due to gain drifts in the MAMA detector or other systematic effects.

Earlier monitoring observations reported evidence for wavelength-dependent lags in the optical/ultraviolet variations in NGC 7469, in the sense that shorter-wavelength variations led

those at longer wavelengths by ∼0.36–1.8 d, with longer lags over longer wavelength baselines. These were explained by differences in light travel times from the central source (that illuminates the disk and drives all the variations) to the hot, inner, ultraviolet-emitting regions and cooler, outer, optical-emitting regions. However, this "reprocessing" model is called into question because it predicts optical interband lags that should have been detected in these observations of NGC 3516, although an definitive statement cannot be made because of the uncertainty in the scaling between NGC 7469 and NGC 3516.

The combination of the lack of X-ray/optical correlation and of lags between optical bands also presents more serious and general difficulties for this reprocessing model, as the sizes indicated by the first point are much larger than the upper limits implied by the second. There are a number of possible model fixes, including anisotropic emission or source geometry, localized flares, or long processing time scales in the disk. However, perhaps the most natural explanation is that the unproven assumption of this reprocessing model, that the X-ray emission powers that at optical/ultraviolet wavelengths, is in error. Clearly, much theoretical work needs to be done to make the reprocessing model fit with this new, emerging picture of Seyfert 1 interband variability.

More observational work is also required: this was an unexpected result in an experiment designed for different purposes. Now that it has been established that *HST* is capable of extremely high precision relative photometry (see also Welsh et al. 1998), it is straightforward to design an experiment expressly to search for very small lags between optical and ultraviolet variations. This can eliminate the inherent uncertainties in comparing model predictions to the data and resolve the ambiguity concerning the relationship between the X-ray through optical variations.

The authors appreciate the fine work of the *RXTE* project, particularly Evan Smith and Tess Jaffe, in scheduling and helping in the reduction of these observations. The authors would also like to thank Andrew Fruchter of STScI for help in scheduling and determining the times of the dithers. This study received financial support from NASA *RXTE* grant NAG 5-7315 and *HST* grant GO-07355. KN acknowledges support from the Universities Space Research Association. BP and SC acknowledge support from NASA LTSA grant NAG 5-8397.

REFERENCES

Beloborodov, A. 1999, ApJL, 510, L123

Chiang, J. et al. 1999, ApJ, submitted, astro-ph/9907114

Clavel, J. & Courvoisier, T. 1991, A & A 248, 389

Clavel, J. et al. 1992, ApJ, 393, 113

Collier, S. et al. 1998, ApJ, 500, 162

Done, C. et al. 1990, MNRAS, 243, 713

Dove, J. et al. 1997, ApJ, 487, 759

Edelson, R., Krolik, J. 1989, ApJ, 333, 646

Edelson, R., Krolik, J., Pike, G. 1990, ApJ, 359, 86

Edelson, R. et al. 1996, ApJ, 470, 364

Edelson, R., Nandra, K. 1999, ApJ, 514, 682

George, I., Fabian, A. 1991, MNRAS 249, 352

Ghisellini, G., Haardt, F., Matt, G. 1994, MNRAS, 267, 743

Golev, V. et al. 1995, MNRAS, 273, 129

Gulibert, P., Rees, M. 1988, MNRAS, 233, 47

Haardt, F., Maraschi, L. 1991, ApJL, 380, L51

Kaspi, S. et al. 1996, ApJ, 470, 336

Korista, K. et al. 1995, ApJS, 97, 285

Kriss, G., Peterson, B. M., Crenshaw, D. M., Zheng, W. 1999, ApJ, submitted, astro-ph/9912204

Krolik, J., Horne, K., Kallman, T., Malkan, M., Edelson, R., Kriss, J. 1991, ApJ, 371, 541

Krolik, J., Madau, P., Zycki, P. 1994, ApJL, 420, L57

Lee, J. et al. 1999, MNRAS, submitted, astro-ph/9909239

Lightman, A., White, T. 1988, ApJ, 335, 57

Maoz, D., Edelson, R., Nandra, K. 1999, AJ, in press, astro-ph/9910023

Nandra, K., George, I., Mushotzky, R., Turner, T. J., Yaqoob, T. 1997, ApJ, 476, 70

Nandra, K. et al. 1998, ApJ, 505, 594

Nandra, K. et al. 1999, ApJL, 523, L17

Peterson, B. M. et al. 1998, PASP, 110, 660

Peterson, B. M., Wandel, A. 1999, ApJL, 521, 95

Pounds, K. et al. 1990, Nature, 344, 132

Press, W. 1978, Comments on Astrophysics, 7, 103

Reynolds, C. 1999, ApJ, in press, astro-ph/9912001

Rokaki, E. et al. 1992, A&A, 253, 57

Shakura, N. & Sunyaev, R. 1973, A&A, 24, 337

Stern, et al. 1995, ApJL, 449, L13

Turner, T. J., George, I., Nandra, K. 1998, ApJ, 508, 648

Turner, T. J. et al. 1999, ApJ, in press, astro-ph/9906050

Wanders, I. et al. 1997, ApJS, 113, 69

Welsh, W., Peterson, B. M., Koratkar, A., Korista, K. 1998, ApJ, 509, 118

White, R., Peterson, B. M. 1994, PASP, 106, 879

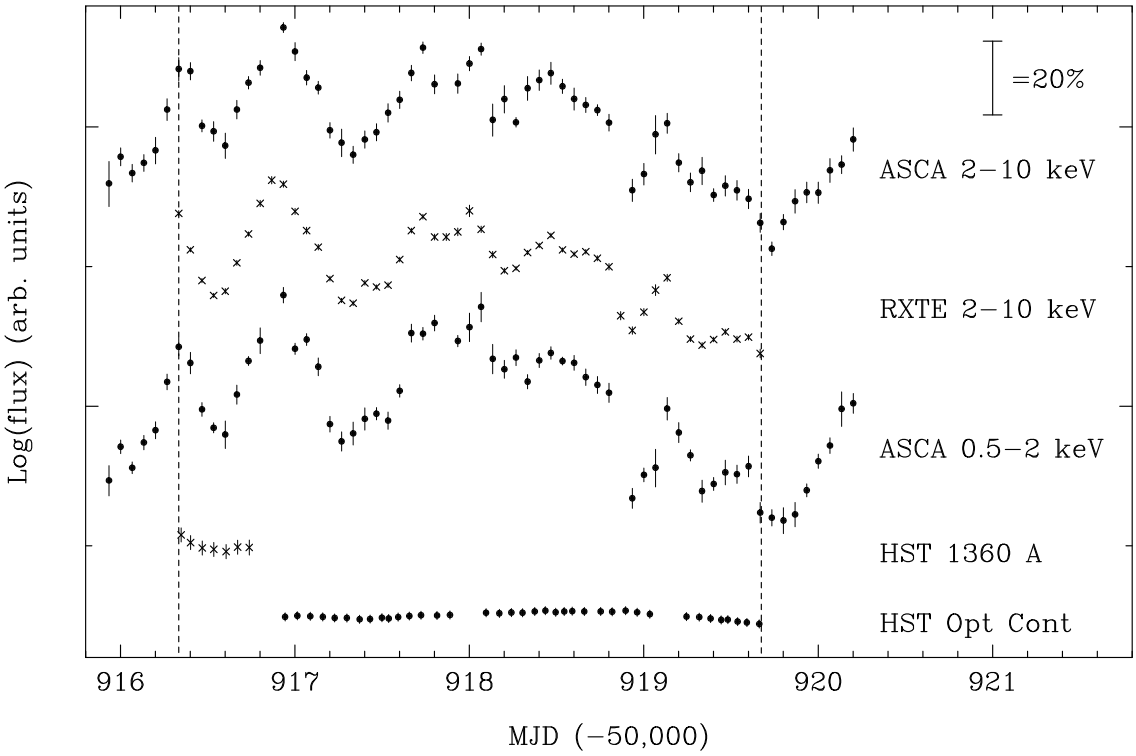

Fig. 1.— X-ray, ultraviolet and optical continuum light curves of NGC 3516. The light curves are, from the top, the *ASCA* hard (2–10 keV) band, the *RXTE* hard (2–10 keV) band, the *ASCA* soft (0.5–2 keV) band, the *HST* ultraviolet (1360 Å) band, and the *HST* mean optical band. The error bar in the upper right shows a factor of 20% change. Error bars are 1σ statistical uncertainties, except for the ultraviolet data, which have 1.7% added in quadrature to account for the systematic errors. Note the strong variability in the X-ray bands, but the ultraviolet and optical variations are quite weak, as shown in detail in Figure 2.

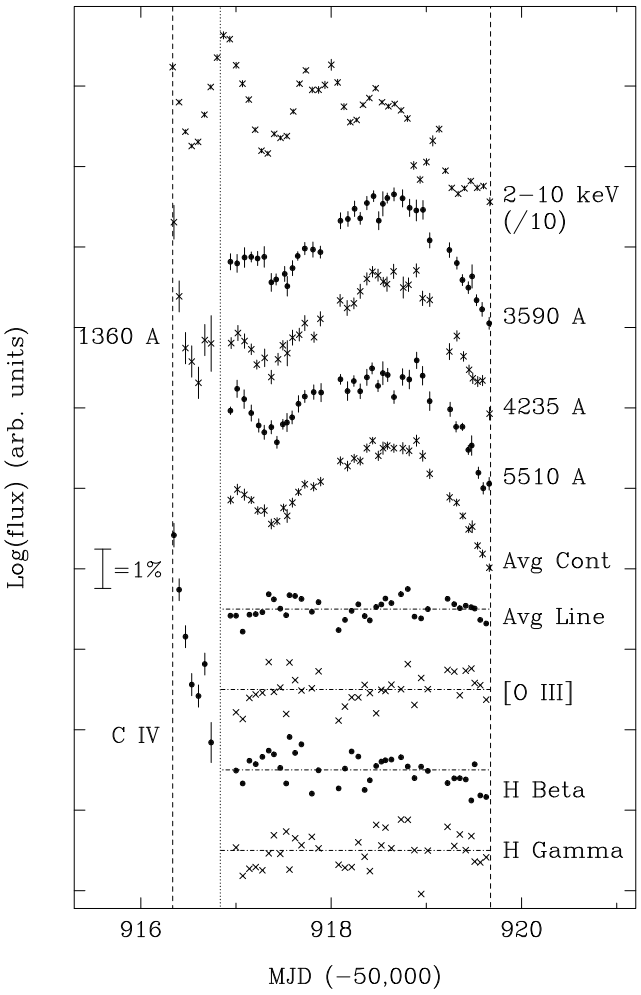

Fig. 2.— Light curves of NGC 3516. At the top is the *RXTE* hard X-ray light curve, scaled down by a factor of 10, for comparison with the *HST* light curves given below. The ultraviolet light curves (left) are for the 1360 Å continuum (top) and C IV emission line (bottom). The optical data (right) are, from the top, 3590 Å, 4235 Å, 5510 Å and average continuum light curves, and the average line, [O III], Hβ and Hγ light curves. The error bars include only statistical errors. The dashed lines denote the beginning and end of the *RXTE* monitoring, and the dotted line separates the UV-MAMA from optical CCD measurements. The horizontal dot-dashed lines show the mean of the emission line light curves. Note specifically that the average optical continuum light curve shows a clear $\sim$2.5% rise followed by a $\sim$3.5% decline. During the same period, the average optical emission line light curve is flat with an RMS scatter of 0.26%, indicating that systematic effects are not likely to be a problem above this level.

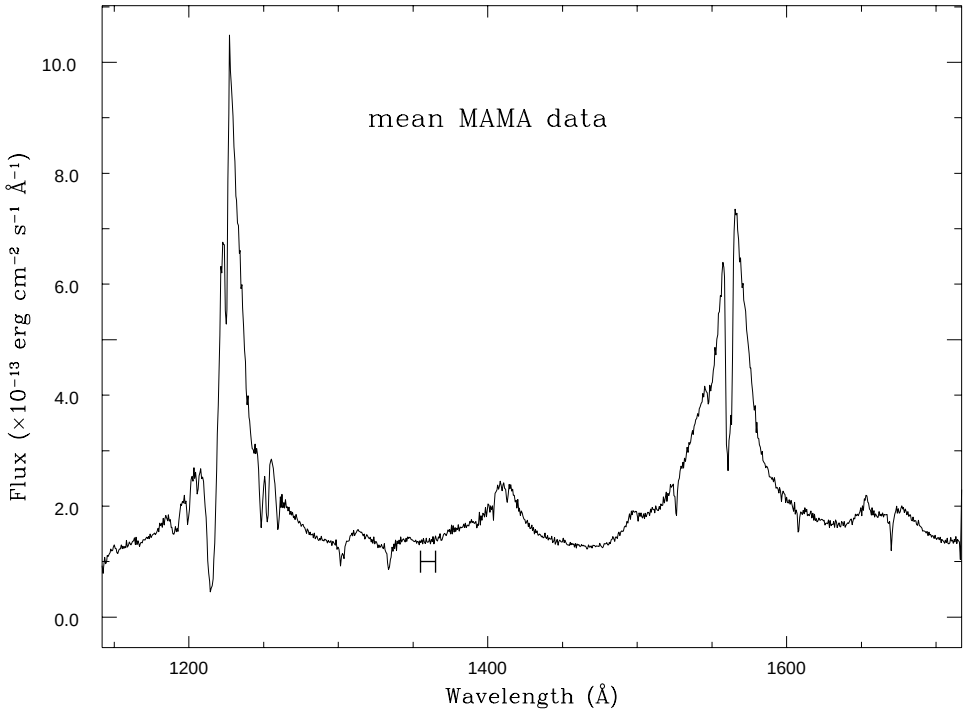

Fig. 3.— Ultraviolet spectrum of NGC 3516. The position of the 1355–1365 Å continuum extraction band is noted by the small horizontal error bar.

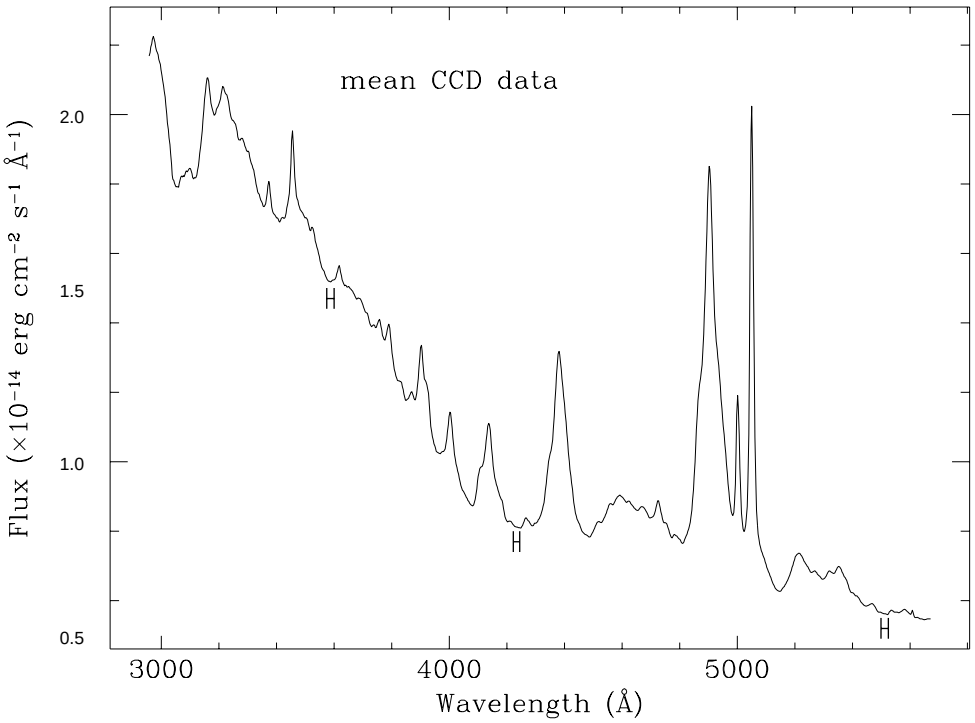

Fig. 4.— Optical spectrum of NGC 3516. Positions of continuum extraction bands (3575–3600 Å, 4223–4245 Å, 5500–5525 Å) are noted by the small horizontal error bars.

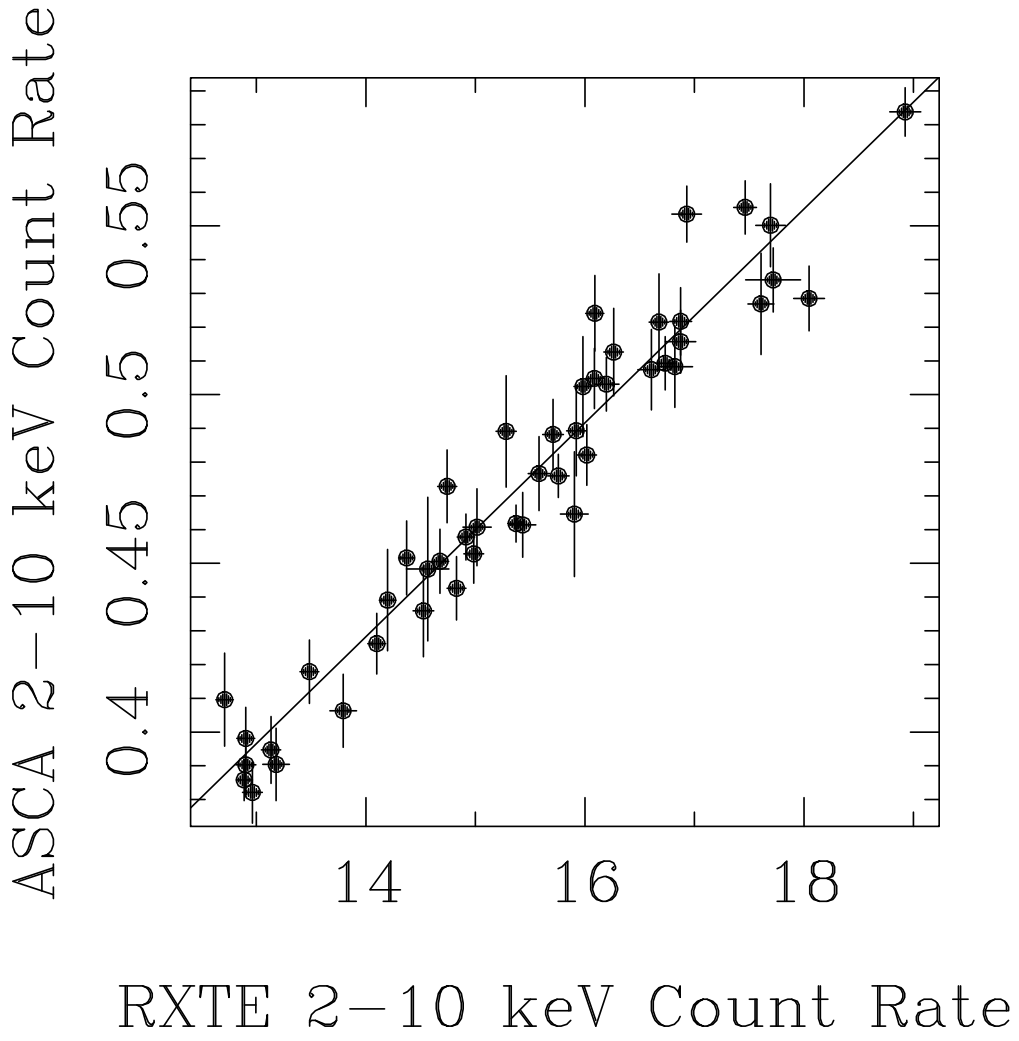

Fig. 5.— Zero-lag correlation plot of 2–10 keV count rates measured from *RXTE* and *ASCA*. The solid line is a linear fit to the data, which goes within 0.5σ of the origin (not shown). Note that the *RXTE* data have much higher count rates, and much better signal-to-noise, than the *ASCA* data.

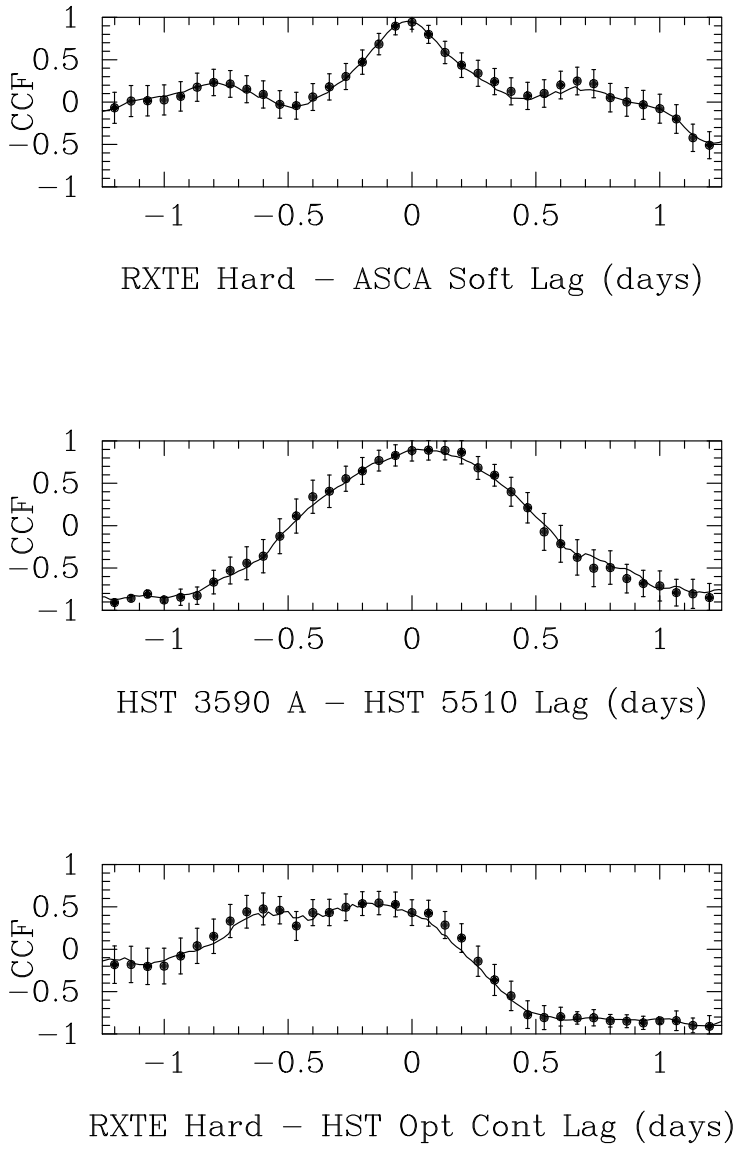

Fig. 6.— Interband temporal cross-correlation functions. The solid line refers to the interpolated cross-correlation function, while the error bars refer to the discrete cross-correlation function. At the top is the *RXTE* hard – *ASCA* soft correlation function, next is the *HST* 3590 Å – 5510 Å correlation function, and at the bottom is the *RXTE* hard – mean optical continuum correlation function. In all plots a negative lag means that the first listed band leads the second.

Table 1. Fractional Variability Levels

Satellite/ Band	Duration (day)	Number of Orbits	Mean Flux	Fractional RMS (%)	Fractional Error (%)	σ_{XS}^2
RXTE 2-10 keV	3.4	51	15[1]	10.81	0.71	0.0114
ASCA 2-10 keV	3.4	48	0.47[1]	11.29	2.28	0.0119
ASCA 0.5-2 keV	3.4	48	0.51[1]	13.45	2.21	0.0172
HST UV 1360 Å Cont	0.4	7	19[2]	1.39	0.45	0.000143
HST UV C IV Line	0.4	7	30[3]	1.80		<0.000277
HST Opt 3590 Å Cont	2.8	38	15[2]	0.86	0.18	0.000069
HST Opt 4235 Å Cont	2.8	38	8.1[2]	0.94	0.17	0.000083
HST Opt 5510 Å Cont	2.8	38	5.6[2]	0.76	0.18	0.000052
HST Opt Avg Cont	2.8	38	8.9[2]	0.82	0.11	0.000066
HST Opt [O III] Line	2.8	38	3.7[3]	0.40		<0.000016
HST Opt Hβ Line	2.8	38	6.4[3]	0.40		<0.000015
HST Opt Hγ Line	2.8	38	2.7[3]	0.44		<0.000019
HST Opt Avg Line	2.8	38	4.0[3]	0.26		<0.000007

Note. — [1]X-ray fluxes (count rates) in ct s^{-1}
[2]*HST* continuum fluxes in 10^{-15} erg cm^{-2} s^{-1} $Å^{-1}$
[3]*HST* line fluxes in 10^{-12} erg cm^{-2} s^{-1}